Chemical Science

EDGE ARTICLE

View Article Online
View Journal | View Issue

Cite this: *Chem. Sci.*, 2015, **6**, 4148

Assessing the exchange coupling in binuclear lanthanide(III) complexes and the slow relaxation of the magnetization in the antiferromagnetically coupled Dy_2 derivative†

Chun Y. Chow,[a] Hélène Bolvin,[b] Victoria E. Campbell,[c] Régis Guillot,[c] Jeff W. Kampf,[a] Wolfgang Wernsdorfer,[d] Frédéric Gendron,[e] Jochen Autschbach,[e] Vincent L. Pecoraro*[a] and Talal Mallah*[c]

Received 21st March 2015
Accepted 7th May 2015

DOI: 10.1039/c5sc01029b

www.rsc.org/chemicalscience

We report here the synthesis and the investigation of the magnetic properties of a series of binuclear lanthanide complexes belonging to the metallacrown family. The isostructural complexes have a core structure with the general formula $[Ga_4Ln_2(shi^{3-})_4(Hshi^{2-})_2(H_2shi^{-})_2(C_5H_5N)_4(CH_3OH)_x(H_2O)_x]\cdot xC_5H_5N\cdot xCH_3OH\cdot xH_2O$ (where H_3shi = salicylhydroxamic acid and Ln = Gd^{III} **1**; Tb^{III} **2**; Dy^{III} **3**; Er^{III} **4**; Y^{III} **5**; $Y^{III}_{0.9}Dy^{III}_{0.1}$ **6**). Apart from the Er-containing complex, all complexes exhibit an antiferromagnetic exchange coupling leading to a diamagnetic ground state. Magnetic studies, below 2 K, on a single crystal of **3** using a micro-squid array reveal an opening of the magnetic hysteresis cycle at zero field. The dynamic susceptibility studies of **3** and of the diluted DyY **6** complexes reveal the presence of two relaxation processes for **3** that are due to the excited ferromagnetic state and to the uncoupled Dy^{III} ions. The antiferromagnetic coupling in **3** was shown to be mainly due to an exchange mechanism, which accounts for about 2/3 of the energy gap between the antiferro- and the ferromagnetic states. The overlap integrals between the Natural Spin Orbitals (NSOs) of the mononuclear fragments, which are related to the magnitude of the antiferromagnetic exchange, are one order of magnitude larger for the Dy_2 than for the Er_2 complex.

Introduction

The design and synthesis of coordination compounds that contain metal centers and combine high spin and magnetic anisotropy have been an active area of research since the discovery of superparamagnetic behavior in the archetypal $[Mn_{12}O_{12}(OCR)_{16}(H_2O)_4]$,[1] the first reported single-molecule magnet (SMM). These molecular magnets are characterized by magnetic bistability and have potential uses in areas such as magnetic data storage, spintronics[2] and quantum computing.[3] A major obstacle to the realization of such applications is the development of molecules with large spin-reversal barriers that will function at practical temperatures. Early efforts towards increasing this barrier involved synthesizing large transition-metal based clusters with high spin ground states.[1,4–6] In order to increase spin, magnetic anisotropy and subsequently, the energy barrier, much of the current SMM research has shifted towards lanthanide based complexes.[7] Due to strong unquenched orbital angular momentum and significant spin–orbit coupling, lanthanide ions possess large intrinsic anisotropy such that mononuclear lanthanide complexes can exhibit slow magnetic relaxation.[8]

Unlike their transition-metal counterparts, lanthanide-based SMMs are at the weak-exchange limit,[9] and have dynamic magnetic behavior which cannot be adequately described within the framework of the zero-field splitting phenomenon,[10] which can be used to understand the origin of the energy barrier in transition-metal SMMs. Furthermore, lanthanide SMMs display dynamic magnetization behavior that can be complicated by the presence of multiple relaxation pathways.[11] Nonetheless, when it comes to designing SMMs with large energy barriers, more metal centers may be better, as it has been shown that metal–metal exchange coupling can aid in suppressing

[a]*Department of Chemistry, University of Michigan, Ann Arbor, Michigan, 48108, USA. E-mail: vlpec@umich.edu*

[b]*Laboratiore de Chimie et Physique Quantiques, Université Toulouse III, 118 route de Narbonne, 31062 Toulouse, France*

[c]*Institut de Chimie Moléculaire et des Matériaux d'Orsay, CNRS, Université de Paris Sud 11, 91405 Orsay Cedex, France. E-mail: talal.mallah@u-psud.fr*

[d]*Institut Néel, CNRS, Université J. Fourier, BP 166 25, Avenue des Martyrs, 38405 Grenoble, France*

[e]*Department of Chemistry, University at Buffalo, State University of New York, Buffalo, NY 14260-3000, USA*

† Electronic supplementary information (ESI) available: Additional magnetic data, additional figures and computational details. CCDC 1020818–1020822. For ESI and crystallographic data in CIF or other electronic format see DOI: 10.1039/c5sc01029b

quantum tunneling phenomena that occur in polynuclear systems.[12] For example, Long and coworkers have shown that a terbium(III) dimer that is strongly coupled through a radical bridge can display hysteresis of a purely molecular origin up to 14 K.[13] Correspondingly, SMMs with some of the largest energy barriers reported to date have been multinuclear lanthanide complexes.[14,15] Unfortunately, due to the radial contraction of 4f orbitals, lanthanide–lanthanide interactions tend to be weak and most polymetallic lanthanide SMMs have magnetic properties which are of single-ion origin;[7] for instance a tetranuclear Dy_4^{III} exhibited barrier heights of 9.7 and 107 K corresponding to two crystallographically independent Dy^{III} sites.[15] In these compounds, the variable temperature ac data show only one distinct relaxation peak indicative of the single-ion relaxation. In order to understand magnetic behavior in complex polynuclear SMMs, simpler model systems are essential for elucidating the underlying 4f–4f interactions.[16,17]

The metallacrown[18] class of supramolecular compounds utilizes versatile ligands which have been used to produce both purely transition-metal and mixed 3d–4f heterometallic SMMs.[4,6,19–21] We employed this synthetic strategy to study lanthanide-only SMMs with the diamagnetic Ga^{III} ion selected to form the backbone of metallacrown complex which isolates the pairs of lanthanide ions, reducing intermolecular dipolar interactions. Herein, we report the synthesis and characterization of an isostructural series of symmetric hexanuclear Ga_4^{III}–Ln_2^{III} compounds with the general formula $[Ga_4Ln_2(shi^{3-})_4(Hshi^{2-})_2(H_2shi^{-})_2(C_5H_5N)_4(CH_3OH)_x(H_2O)_x]\cdot x C_5H_5N\cdot x CH_3OH\cdot x H_2O$ (Ln^{III} = Gd^{III} **1**, Tb^{III} **2**, Dy^{III} **3**, Er^{III} **4**, Y^{III} **5**, $Y^{III}_{0.9}Dy^{III}_{0.1}$ **6**), where the dimeric lanthanide Ln_2O_2 unit is protected by the Ga_4 ring, thus precluding large dipolar intermolecular interactions. To date, compound **3** is a rare example of an antiferromagnetically coupled Ising-like lanthanide dimer with a diamagnetic ground state that shows an opening of the hysteresis loop at zero magnetic field, a behavior that was also observed in the antiferromagnetically coupled Dy_3 complexes.[22]

Experimental section

General information

All reagents and chemicals were purchased from Sigma Aldrich or Alfa Aesar and were used without further purification. All reactions were carried out under aerobic conditions. Elemental analysis was performed by Atlantic Microlabs Inc. All reactions were carried under aerobic conditions.

Synthesis of Gd_2Ga_4 (1)

Salicylhydroxamic acid (153.1 mg, 1.000 mmol), $Gd(NO_3)_3\cdot 6H_2O$ (112.8 mg, 0.2500 mmol), $Ga(NO_3)_3\cdot xH_2O$ (127.9 mg, 0.5000 mmol) were dissolved in 46 mL methanol. 13 mL pyridine was added drop wise to this solution, followed by 6.5 mL H_2O. The solution was stirred for 30 seconds and then filtered. Slow evaporation of half of the solution yielded crystalline compound after 2 weeks.

Synthesis of Tb_2Ga_4 (2), Dy_2Ga_4 (3), Er_2Ga_4 (4) and Y_2Ga_4 (5)

A general procedure for complexes **2**, **3**, **4** and **5** is as follows. Salicylhydroxamic acid (153.1 mg, 1.000 mmol), $Ln(NO_3)_3\cdot xH_2O$ (0.2500 mmol), $Ga(NO_3)_3\cdot xH_2O$ (127.9 mg, 0.5000 mmol) were dissolved in 21 mL methanol. 6 mL pyridine was added drop wise to this solution, followed by 3 mL H_2O. The solution was stirred for 30 seconds and then filtered. Slow evaporation of half of the solution yielded crystalline compound after 2 weeks.

Synthesis of $Y_{1.8}Dy_{0.2}Ga_4$ (6)

Salicylhydroxamic acid (153.1 mg, 1.000 mmol), $Dy(NO_3)_3\cdot 5H_2O$ (11.0 mg, 0.0250 mmol), $Y(NO_3)_3\cdot 5H_2O$ (82.1 mg, 0.225 mmol), $Ga(NO_3)_3\cdot xH_2O$ (127.9 mg, 0.5 mmol) were dissolved in 21 mL methanol. 6 mL pyridine was added drop wise to this solution, followed by 3 mL H_2O. The solution was stirred for 30 seconds and then filtered. Slow evaporation of half of the solution yielded crystalline compound after 2 weeks.

$[Ga_4Gd_2(shi^{3-})_4(Hshi^{2-})_2(H_2shi^{-})_2(C_5H_5N)_4(CH_3OH)_{0.69}(H_2O)_{1.31}]\cdot 3C_5H_5N\cdot 2.31CH_3OH\cdot 3H_2O$ (1).‡. Yield: 0.0850 g (26.9%), anal. calcd for $Gd_2Ga_4C_{94}H_{93.62}N_{15}O_{31.31}$: C, 44.66; H, 3.73; N, 8.31. Found: C, 43.94; H, 3.64; N, 8.37. Single-crystal unit cell: monoclinic, space group *C*2/*c*, a = 25.2329 Å, b = 22.0543 Å, c = 17.9967 Å, α = 90.0000° β = , 99.090°, γ = 90.0000°, V = 10 043.9599 Å^3.

$[Ga_4Tb_2(shi^{3-})_4(Hshi^{2-})_2(H_2shi^{-})_2(C_5H_5N)_4(CH_3OH)(H_2O)]\cdot 3C_5H_5N\cdot 2CH_3OH\cdot 3H_2O$ (2). Yield: 0.0892 g (28.3%), anal. calcd for $Tb_2Ga_4C_{94}H_{93}N_{15}O_{31}$: C, 44.70; H, 3.71; N, 8.32. Found: C, 44.45; H, 3.63; N, 8.38. Single-crystal unit cell: monoclinic, space group *C*2/*c*, a = 25.1697 Å, b = 22.1217 Å, c = 17.9895 Å, β = 99.302°, V = 9884.8 Å^3.

$[Ga_4Dy_2(shi^{3-})_4(Hshi^{2-})_2(H_2shi^{-})_2(C_5H_5N)_4(CH_3OH)(H_2O)]\cdot 3C_5H_5N\cdot 2CH_3OH\cdot 3H_2O$ (3). Yield: 0.1291 g (40.8%), anal. calcd for $Dy_2Ga_4C_{94}H_{93}N_{15}O_{31}$: C, 44.58; H, 3.70; N, 8.30. Found: C, 44.76; H, 3.41; N, 8.38. Single-crystal unit cell: monoclinic, space group *C*2/*c*, a = 25.1638 Å, b = 22.1781 Å, c = 18.0649 Å, β = 99.353°, V = 9947.72 Å^3.

$[Ga_4Er_2(shi^{3-})_4(Hshi^{2-})_2(H_2shi^{-})_2(C_5H_5N)_4(CH_3OH)(H_2O)]\cdot 3C_5H_5N\cdot 1CH_3OH\cdot 4H_2O$ (4). Yield: 0.0947 g (29.8%), anal. calcd for $Er_2Ga_4C_{93}H_{91}N_{15}O_{31}$: C, 44.18; H, 3.63; N, 8.31. Found: C, 44.28; H, 3.58; N, 8.49. Single-crystal unit cell: monoclinic, space group *C*2/*c*, a = 25.1476 Å, b = 22.1380 Å, c = 18.0285 Å, α = 90.0000° β = 99.1768°, γ = 90.0000°, V = 9908.3211 Å^3.

$[Y_2Ga_4(shi^{3-})_4(Hshi^{2-})_2(H_2shi^{-})_2(C_5H_5N)_4(CH_3OH)(H_2O)]\cdot 3C_5H_5N\cdot 2CH_3OH\cdot 3H_2O$ (5). Yield: 0.160.7 g (53.9%), anal. calcd for $Y_2Ga_4C_{94}H_{93}N_{15}O_{31}$: C, 47.33; H, 3.93; N, 8.81. Found: C, 47.54; H, 3.75; N, 8.86. Single-crystal unit cell: monoclinic, space group *C*2/*c*, a = 25.1053 Å, b = 22.1794 Å, c = 18.0733 Å, α = 90.000° β = 99.377°, γ = 90.000°, V = 9929.11 Å^3.

$[Ga_4Y_{1.8}Dy_{0.2}(shi^{3-})_4(Hshi^{2-})_2(H_2shi^{-})_2(C_5H_5N)_4(CH_3OH)(H_2O)]\cdot 3C_5H_5N\cdot 2CH_3OH\cdot 3H_2O$ (6). Yield: 0.1363 g (45.4%), anal. calcd for $Y_{1.8}Dy_{0.2}Ga_4C_{94}$ $H_{93}N_{15}O_{31}$: C, 47.04; H, 3.91; N, 8.75. Found: C, 46.82; H, 3.76; N, 8.94. Single-crystal unit cell: monoclinic, space group *C*2/*c*, a = 25.1476 Å, b = 22.1380 Å, c = 18.0285 Å, α = 90.0000° β = 99.1768°, γ = 90.0000°, V = 9908.3211 Å^3.

Table 1 Crystallographic details for the analogous $[Ga^{III}_4Ln^{III}_2(shi^{3-})_4(Hshi^{2-})_2(H_2shi^{-})_2(C_5H_5N)_4(CH_3OH)(H_2O)]$ complexes

	1	2	3	4	5
Mol formula	$Ga_4Gd_2C_{94}H_{93.62}N_{15}O_{31.31}$	$Ga_4Tb_2C_{94}H_{93}N_{15}O_{31}$	$Ga_4Dy_2C_{94}H_{93}N_{15}O_{31}$	$Ga_4Er_2C_{93}H_{91}N_{15}O_{31}$	$Ga_4Y_2C_{94}H_{93}N_{15}O_{31}$
fw (g mol^{-1})	2527.80	2525.55	2532.71	2528.21	2385.53
Cryst syst/space group	Monoclinic, *C*2/*c*	Monoclinic, *C*2/*c*	Monoclinic, *C*2/*c*	Monoclinic, *C*2/*c*	Monoclinic, *C*2/*c*
T (K)	85(2)	100(1)	85(2)	85(2)	85(2)
Wavelength (Å)	0.71073	0.71073	1.54178	1.54178	1.54178
a (Å)	25.233(5)	25.1697(6)	25.1638(18)	25.1476(5)	25.1053(18)
b (Å)	22.054(4)	22.1217(6)	22.1781(4)	22.1380(4)	22.1794(4)
c (Å)	17.997(4)	17.9895(5)	18.0649(3)	18.0285(13)	18.0733(3)
α (deg)	90	90	90	90	90
β (deg)	99.09(3)	99.3020(10)	99.353(7)	99.177(7)	99.377(7)
γ (deg)	90	90	90	90	90
V (Å^3)	9889.3(3)	9884.8(5)	9947.7(8)	9908.3(8)	9929.1(8)
Z	4	4	4	4	4
Density, ρ (g cm^{-3})	1.698	1.697	1.691	1.695	1.596
Abs coeff., μ (mm^{-1})	2.486	2.462	9.839	4.949	3.460
F(000)	5060	5056	5063	5048	4848
θ range for data collection (deg)	1.59–25.44	1.59–30.67	3.44–68.23	3.45–68.24	3.44–68.25
Limiting indices	$-30 \le h \le 30$, $-26 \le k \le 26$, $-21 \le l \le 21$	$-30 \le h \le 36$, $-31 \le k \le 31$, $-25 \le l \le 25$	$-27 \le h \le 29$ $-26 \le k \le 26$ $-21 \le l \le 21$	$-30 \le h \le 30$, $-26 \le k \le 26$, $-21 \le l \le 21$	$-30 \le h \le 30$, $-26 \le k \le 25$, $-21 \le l \le 21$
Reflns collected/unique	76 042/9136	152 738/15 061	133 023/9072	139 170/9069	140 855/9097
Completeness to θ (%)	99.8	99.2	99.5	99.9	100.0
No. of data/restraints/params	9136/128/745	15 061/70/750	9072/92/746	9069/76/741	9097/175/744
Goodness of fit on F^2	1.075	1.130	1.031	1.100	1.103
Final *R* indices [$I > 2\sigma(I)$]	$R_1{}^a = 0.0422$ $wR_2{}^b = 0.1051$	$R_1{}^a = 0.0372$ $wR_2{}^b = 0.0814$	$R_1{}^a = 0.0572$ $wR_2{}^b = 0.1545$	$R_1{}^a = 0.0868$ $wR_2{}^b = 0.2382$	$R_1{}^a = 0.0437$ $wR_2{}^b = 0.1221$
R Indices (all data)	$R_1{}^a = 0.0616$ $wR_2{}^b = 0.1206$	$R_1{}^a = 0.0657$ $wR_2{}^b = 0.0980$	$R_1{}^a = 0.0627$ $wR_2{}^b = 0.1591$	$R_1{}^b = 0.0957$ $wR_2{}^a = 0.2574$	$R_1{}^a = 0.0459$ $wR_2{}^b = 0.1238$
Largest diff peak and hole (e$^-$ Å^{-3})	1.657 and −0.742	1.467 and −0.899	1.792 and −1.514	2.175 and −0.899	0.942 and −0.745

^{a} $R_1 = \Sigma(||F_o| - |F_c||)/\Sigma|F_o|$. ^{b} $wR_2 = [\Sigma[w(F_o{}^2 - F_c{}^2)^2]/\Sigma[w(F^\circ)^2]]^{1/2}$; $w = 1/[\sigma^2(F_o{}^2) + (mp)^2 + np]$; $p = [\max(F_o{}^2,0) + 2F_c{}^2]/3$ (*m* and *n* are constants); $\sigma = [\Sigma[w(F_o{}^2 - F_c{}^2)^2]/(n-p)]^{1/2}$.

Single-crystal X-ray diffraction

Crystal data for compound **1** were collected at 85(2) K on a Bruker SMART-APEX CCD-based X-ray diffractometer equipped with a low temperature device and fine-focus Mo-target X-ray tube ($\lambda = 0.71073$ Å), operated at 1500 W power (50 kV, 30 mA). The frames were integrated with the Bruker SAINT[23] software package with a narrow frame algorithm. The data were processed with SADABS[24] and corrected for absorption.

Crystal data for compound **2** were collected on a Kappa X8 APPEX II Bruker diffractometer with graphite-monochromated Mo Kα radiation (= 0.71073 Å). Crystals were mounted on a CryoLoop (Hampton Research) with Paratone-N (Hampton Research) as cryoprotectant and then flashfrozen in a nitrogen-gas stream at 100 K. The temperature of the crystal was maintained at the selected value (100 K) by means of a 700 series Cryostream cooling device to within an accuracy of ±1 K. The data were corrected for Lorentz polarization, and absorption effects.

Crystal data for compounds **3**, **4** and **5** were collected at 85(2) K on an AFC10K Saturn 944+ CCD-based X-ray diffractometer equipped with a Micromax007HF Cu-target microfocus rotating anode ($\lambda = 1.54187$ Å), operated at 1200 W power (40 kV, 30 mA). The data were processed with CrystalClear 2.0 and corrected for absorption.[25]

All structures were solved and refined with the SHELXTL (version 6.12) software package.[26] All non-hydrogen atoms were refined anisotropically. Hydrogen atoms are placed in their idealized positions. Additional details are provided in Table 1.

Magnetic measurements

Variable-temperature susceptibility, variable-field magnetization and ac susceptibility measurements on polycrystalline samples mulled in eicosane were performed on a Quantum Design MPMS SQUID magnetometer. Variable-temperature dc susceptibility measurements were performed at 2000 Oe from 2–300 K. Isothermal magnetization measurements were performed at 2 K from 0–7 T. AC magnetic susceptibility measurements were done at both zero and applied fields (2000 Oe for **3** and 750 Oe for **6**) with an ac drive field of 3 Oe at frequencies ranging from 1 to 1488 Hz. Dc susceptibilities were corrected for the sample holder and eicosane and for diamagnetism of constituent atoms using Pascal's constants.

Micro-SQUID measurements

Magnetization measurements on oriented single crystals were carried out with an array of micro-SQUIDs.[27] The field aligned parallel to the easy-axis of magnetization by the transversal field method.[28] Measurements were performed at a temperature range from 0.03 to 5 K in fields up to 1.1 T with sweep rates between 0.008 and 0.280 T s^{-1}.

Computational details

Calculations are performed within the crystallographic geometry on the binuclear species where one lanthanide has been replaced by a Lu^{III} diamagnetic ion. Magnetic properties are calculated using first principle methods on a monomeric species by replacing one of the lanthanide by a diamagnetic lutetium of configuration $4f^{14}$. Since the two lanthanide atoms are related by an inversion center, there is only one type of monomer. All atoms are described with all electron basis sets ANO-RCC,[29] Ln atoms with TZP quality, N and O atoms with DZP quality and other atoms with DZ quality. The excited states of the complexes have been calculated with the SO-CASSCF method using the MOLCAS78 suite of programs (MOLCAS80 for the gadolinium complex).[30] The active space consists of n electrons in the 7 4f orbitals for an atom of configuration $4f^n$. First, a CASSCF (Complete Active Space Self Consistent Field) calculation is performed:[31] all the states with the maximal value of the spin are considered in the state average procedure. In the case of gadolinium, all the sextet states are considered in addition to the octuplet ground state. Spin–orbit coupling is evaluated as a state interaction between all CASSCF wave functions by the RASSI (Restricted Active Space State Interaction) method.[32] Spin–Orbit (SO) integrals are evaluated within the AMFI approximation.[33] The calculation of all the properties is implemented in a local program. *g* factors are calculated according to ref. 34 even in the case of non-degenerate states (see ESI† for details). The dipolar magnetic interaction is calculated as

$$\hat{H}^{\mathrm{dip}} = \frac{\mu_0}{4\pi R^3}\left\{ \hat{\vec{M}}^{\mathrm{A}} . \hat{\vec{M}}^{\mathrm{B}} - 3\hat{M}_z^{\mathrm{A}}\ \hat{M}_z^{\mathrm{B}} \right\}$$

where R is the intermetallic distance, z the intermetallic direction and μ_0 the magnetic constant. The exchange interactions are carried by the spin densities and are described by a Heisenberg–Dirac–Van Vleck (HDVV) Hamiltonian

$$\hat{H}^{\mathrm{Heis}} = -J\ \hat{\vec{S}}^{\mathrm{A}} \cdot \hat{\vec{S}}^{\mathrm{B}}$$

$\hat{\vec{M}}^{\mathrm{A(B)}}$ and $\hat{\vec{S}}^{\mathrm{A(B)}}$ are the total and spin momentum operators for site A(B). This scheme has been first proposed by Lines in the 70 s,[35] it has been applied to lanthanide complexes by Sutter *et al.* in 2002 (ref. 36) and since 2007, is applied in the group of Chibotaru[37] A local modification of MOLCAS was used to generate natural spin orbitals (NSOs) from SO-CASSCF calculations[38] (see ESI†).

Results and discussion

Synthesis and characterization

The flexible multidentate ligand salicylhydroxamic acid (H_3shi) has been used in the synthesis of numerous metallacrown complexes,[18] including several single-molecule magnets.[6,20,21] Both predictable structure types (such as 9-MC-3, 12-MC-4) as well as compounds with unpredictable molecular geometry can be synthesized with H_3shi by adjusting reaction and solvent conditions, allowing for isolation and study of a wide array of multinuclear metallacrown complexes. Pyridine (which acts as a base, a solvent and a ligand) has unique properties, which have resulted in several metallacrown complexes with both previously known and new structure types.[21,39] This multipurpose

solvent aids in crystallization by forming π-interactions and coordinates to metal sites, forming structures whose architectures are directed by π-interactions and steric effects. Here, the reaction of H_3shi, $Ga(NO_3)_3 \cdot xH_2O$ and $Ln(NO_3) \cdot xH_2O$ a 4 : 2 : 1 stoichiometric ratio in a solution of methanol, pyridine and water followed by slow evaporation of solvent afforded neutral macrocyclic complexes (Scheme 1) with the general formula $[Ga_4Ln_2(shi^{3-})_4(Hshi^{2-})_2(H_2shi)_2(C_5H_5N)_4(CH_3OH)(H_2O)] \cdot 3C_5H_5N \cdot 2CH_3OH \cdot 3H_2O$. The structures of compounds **1–5** were determined by X-ray crystallography to be isostructural and crystallize in the monoclinic *C*2/*c* space group (Table 1). Slight differences in the composition of bound and lattice solvents were observed across the series of complexes. Compound **6** was determined to have the same unit cell parameters and is isostructural to **3** and **5** (Y_2Ga_4). It was synthesized with 10% Dy^{III} and 90% Y^{III} in solution. Statistically speaking, such a reaction would form crystals composed of 81% Y_2Ga_4 (diamagnetic), 18% $DyYGa_4$ and 1% Dy_2Ga_4 (**3**).

As a representative example, the structure of compound **3** (Fig. 1) can be described as a centrosymmetric μ_2-oxo bridged di-lanthanide core surrounded by four peripheral Ga^{III} ions. In the core moiety of the asymmetric unit, one Dy^{III} and two Ga^{III} ions are chelated by four fully and partially deprotonated ligands and coordinated by pyridine and methanol or water solvent molecules. In Fig. 1, Dy1 is chelated by the carbonyl (O1) and hydroximate oxygens (O2) of an in-plane shi^{3-} and by the carbonyl (O7) and phenoxide oxygens of an out-of-plane $Hshi^{2-}$.

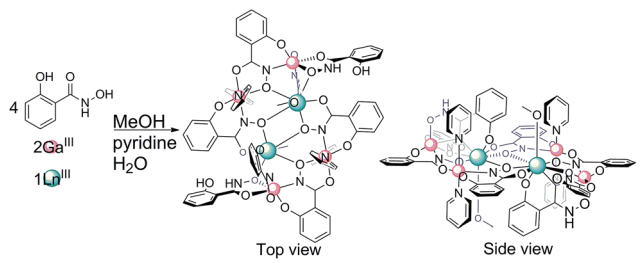

Ln^{III} = Gd^{III} (**1**), Tb^{III} (**2**), Dy^{III} (**3**), Er^{III} (**4**), Y^{III} (**5**), $Y^{III}_{0.9}Dy^{III}_{0.1}$ (**6**)

Scheme 1 Synthesis of Ln_2Ga_4 complexes.

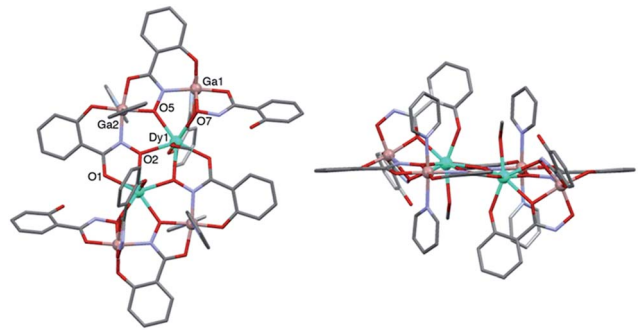

Fig. 1 X-ray crystal structure of complex 3. (left) Top view. (right) Side view. Color code: teal spheres = Dy^{III}; salmon spheres = Ga^{III}; gray = C; red = O; blue = N. Hydrogen atoms and lattice solvents are omitted for clarity.

The symmetry-generated hydroximate oxygen O2a also coordinates to Dy1, to form a $Dy_2(\mu_2\text{-}OR)_2$ core. Hydroximate oxygens from an in-plane shi^{3-} (O5) and $Hshi^{2-}$ (O11) also coordinate, bridging Dy1 to Ga2a and Ga1, respectively. Dy1 is capped by a disordered water (O510) or methanol (O500, C500) with shared occupancy, to complete the coordination sphere around Dy1 which can be described as having distorted 8-coordinate trigonal dodecahedral geometry (Table S1†). The four outer Ga^{III} cations, with roughly octahedral geometry, surround the two central Dy^{III} ions and are ligated by fully and partially deprotonated H_3shi. Four fully deprotonated shi^{3-} and two H_2shi^{-} coordinate the four Ga^{III} and two Dy^{III} ions to form the molecular plane (Fig. 1, left), with two doubly deprotonated $Hshi^{2-}$ pointing above and below the plane (Fig. 1, right).

Static magnetic studies and theoretical calculations

For complexes, the variable-temperature dc susceptibility measurements were performed at an applied field of 2000 Oe from 2 to 300 K (Fig. S3†).; the variable-field magnetization measurements were performed at 2 K from 0 to 7 T (Fig. S3†). Globally, the general behavior of all compounds is consistent with other lanthanide complexes reported in the literature.[17,22,40]

Gd_2Ga_4 1

The room temperature χT value for **1** (Gd^{III}: $^8S_{7/2}$, 15.9 $cm^3\ K\ mol^{-1}$) is in good agreement with the expected value for two non-interacting Gd^{III} ions. Upon cooling, χT is almost constant down to $T = 10$ K and then slightly decreases to reach a value of 7.8 $cm^3\ mol^{-1}$ K at 2 K. This decrease is probably due to an intramolecular antiferromagnetic exchange coupling between the two Gd^{III} ions. The $M = f(\mu_0 H)$ curve increases with the applied magnetic field and reaches saturation (13.8 Bohr Magneton) at 7 T. It is possible to fit the susceptibility and the magnetization data (see Fig. 2 and 3) using a model based on

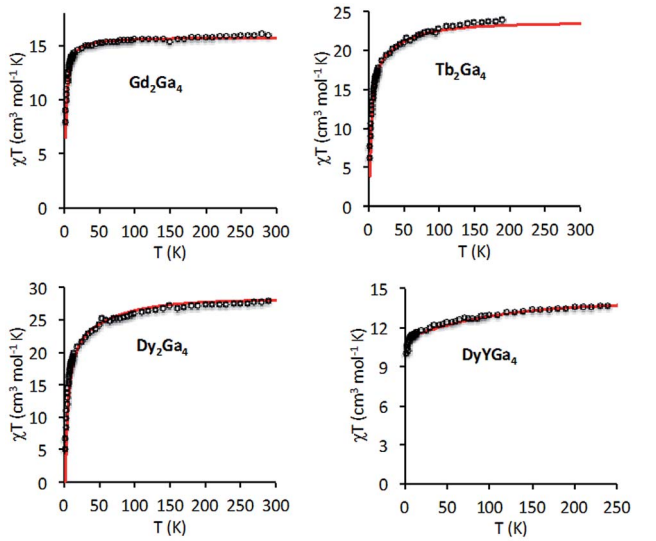

Fig. 2 Temperature dependence of the χT product for complexes **1**, **2**, **3** and **6**. The solid lines correspond to the best fit (see text).

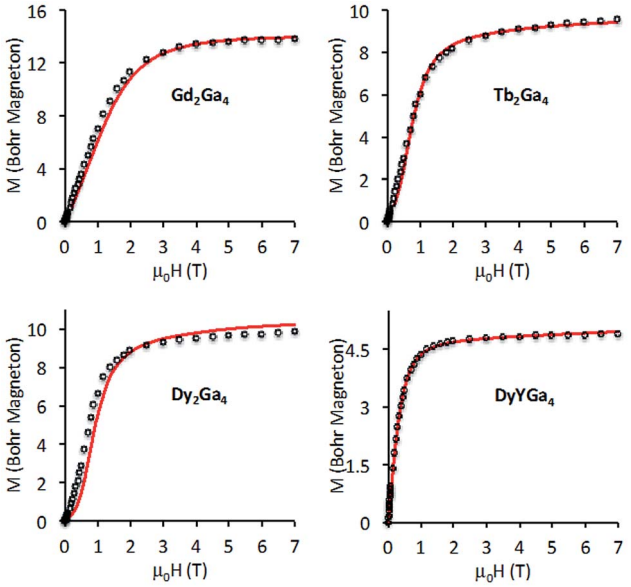

Fig. 3 Magnetization *vs.* applied field at 2 K for complexes **1**, **2**, **3** and **6**. The solid lines correspond to the best fit (see text).

the spin Hamiltonian $H = -JS_{Gd1} \times S_{Gd2} + g\beta H_z S_z$. The best fit parameters are $g = 1.98$ and $J = -0.16$ cm^{-1}, where g is the Lande factor and J the interaction parameter between the local $S = 7/2$ spins of the Gd^{III} ions. This value is in agreement with those reported in the literature for a dinuclear μ-oxo Gd^{III} with a similar geometry.[41] The Gd^{III} ion has no first order angular momentum and almost a negligible zero field splitting. In such a case, the dipolar interaction is expected to be very weak. Thus, the antiferromagnetic interaction found experimentally is due, mainly, to exchange and splits the low-lying spin states $S = 0$ to 7 by an energy equal to 4.48 cm^{-1} ($JS(S + 1)/2$), with $|J| = 0.16$ cm^{-1} and $S = 7/2$ (see Table S2 and S3†).§

Tb_2Ga_4 2, Dy_2Ga_4 3 and $DyYGa_4$ 6

The χT product and the field dependent magnetization at 2 K for **6** (Fig. 2 and 3) have the behavior expected for a mononuclear Dy^{III} complex ($^6H_{15/2}$, $C = 14.17$ cm^3 K mol^{-1}). *Ab initio* calculations allows for the determination of the energy spectrum and the associated g_i values (Table S4†) ($i = 1$, 2 and 3 are the principal directions of the g tensor with 1 corresponding to the largest value). The ground state corresponds to $M_J = \pm 15/2$, with one very large $g_1 = 19.85$ ($g_2 = 0.08$, $g_3 = 0.04$),¶ indicating an easy axis of the magnetization as depicted in Fig. 4 (left). The magnetization axis forms an angle of 79° with the Dy–Dy axis and is very close to the plane containing the Dy^{III} ions and the bridging oxygen atoms. The experimental magnetic data can be reproduced using the M_J energy spectrum determined from *ab initio* calculations, which confirms the nature of the ground level ($M_J = \pm 15/2$) and the fact that the diluted compound mainly contains the paramagnetic $DyYGa_4$ species.

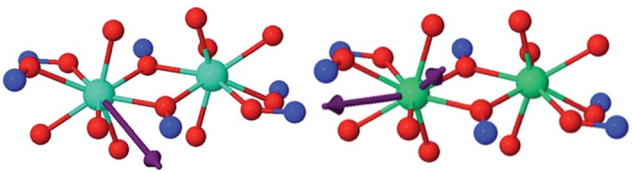

Fig. 4 (left) Orientation of the magnetization axis of the ground Kramers doublet $M_J = \pm 15/2$ of the Dy^{III} ion in **6** where one Dy^{III} has been replaced by a Lu^{III} ion. (right) Orientation of the two components of the easy plane of magnetization for the ground Kramers doublet of Er^{III} ion in **5** where one Er^{III} has been replaced by a Lu^{III} ion.

The χT product for **2** and **3** have the usual behavior expected for Tb^{III} and Dy^{III} ions ($^7F_6$ ground state $C = 11.82$ cm^3 mol^{-1} K for an isolated Tb^{III}); it slowly diminishes from 300 K to around 50 K and then decreases more abruptly. This behavior is due to the thermal depopulation of excited M_J sublevels and may also be caused by an antiferromagnetic interaction between the lanthanide ions. The magnetization measured at 2 K presents a sigmoidal shape at low applied magnetic fields with an inflection point around 0.5 T, which is the signature of the presence of an antiferromagnetic coupling within the two compounds. It is worth noting that the magnetization *vs.* field curve of **6** does not possess an inflection point and its χT product value at 2 K (10.8 cm^3 mol^{-1} K) is larger than that of **3** (2.6 cm^3 mol^{-1} K computed per 1 Dy^{III}), which confirms that the inflection point in **3** is due to *intra-* and not to *inter*molecular antiferromagnetic interaction. In order to determine the value of the inflection point more accurately in the $M = f(\mu_0 H)$ curve, we measured the magnetization at very low temperature on a single crystal of **3** using an array of micro-squids with the magnetic field parallel to the anisotropy axis of the crystal. The curves at $T = 1$ and 0.03 K show sharp steps and a crossing point at $\mu_0 H = 0.51$ T (Fig. S1†).

The sharp steps are the result of the crossover from an antiparallel (antiferromagnetic: AF) to a parallel (ferromagnetic: F) alignment of the anisotropic moments of the two Dy^{III} ions. The field value of the crossing point allows for computation of the energy difference ΔE ($\Delta E = g_1 \times \beta \times \mu_0 H = 19.47 \times 0.496 \times 0.51$) between the AF and the F states and was found equal to 4.9 cm^{-1}. The magnetic dipolar interaction between the two Dy^{III} ions (Table S5†), determined by *ab initio* calculations of the isolated ion shows that the minimum energy is obtained when the magnetization moments are antiparallel, which is expected because the easy magnetization axis is almost perpendicular to the Dy–Dy axis. These calculations lead to an AF–F energy gap of 1.26 cm^{-1} well below the experimental one extracted from the magnetization data (4.9 cm^{-1}). In order to account for the experimental energy gap, we introduced an additional interaction due to an exchange coupling between the two Dy^{III} ions (see Experimental section). A good fit of the data of **3** is obtained using a J_{exc} value of −0.29 cm^{-1} (Fig. 3, S1 and Table S5†). The difference between the calculated and the experimental data at low temperature (Fig. S1†) is the signature of intermolecular dipolar interaction within the crystal that can be observed at such low temperatures.

For the Tb complex **2**, the situation is similar to that of the Dy analogue; an easy axis of magnetization is present, where $g_1 = 17.85$ and $g_2 = g_3 = 0$ for the $M_J = \pm 6$ ground levels (Table S6, see ESI†). It forms an angle of 79° with the Tb–Tb intermetallic

axis (Fig. S2†). The computed dipolar interaction leads to a splitting between the AF (ground level) and the F states of 0.5 cm^{-1}, which is not sufficient to reproduce the experimental data (Table S7†). Introducing an additional antiferromagnetic exchange interaction, $2|J|M_S^2$ ($J = -0.12$ cm^{-1}), increases this energy by 2.7 cm^{-1} and affords a reasonable fit of the data (Fig. 3 and Table S7†).

Er_2Ga_4 5

The χT value at room temperature (22.7 cm^3 mol^{-1} K) corresponds to two isolated Er^{III} ions (Er^{III}: $^4I_{15/2}$, $C = 11.5$ cm^3 K mol^{-1}) (Fig. S3†). Upon cooling, χT slightly decreases and reaches a value of 12.9 cm^3 K mol^{-1} at 2 K, as expected for anisotropic ions. The $M = f(\mu_0 H)$ curve increases sharply between 0 and 1 T and then continuously up to 7 T without reaching saturation (Fig. S3†).

No inflection point is present at low magnetic field, which excludes the presence of an antiferromagnetic coupling as for the other compounds. For the ground state, the *ab initio* calculations give three different g values: $g_1 = 9.94$, $g_2 = 5.25$ and $g_3 = 0.25$ (Table S8†). The magnetization is planar, with two non-equivalent directions. The largest magnetization direction (along g_1) is found in a direction forming an angle of 32° with the intermetallic axis and lies almost in the Er_2O_2 plane (Fig. 4, right).

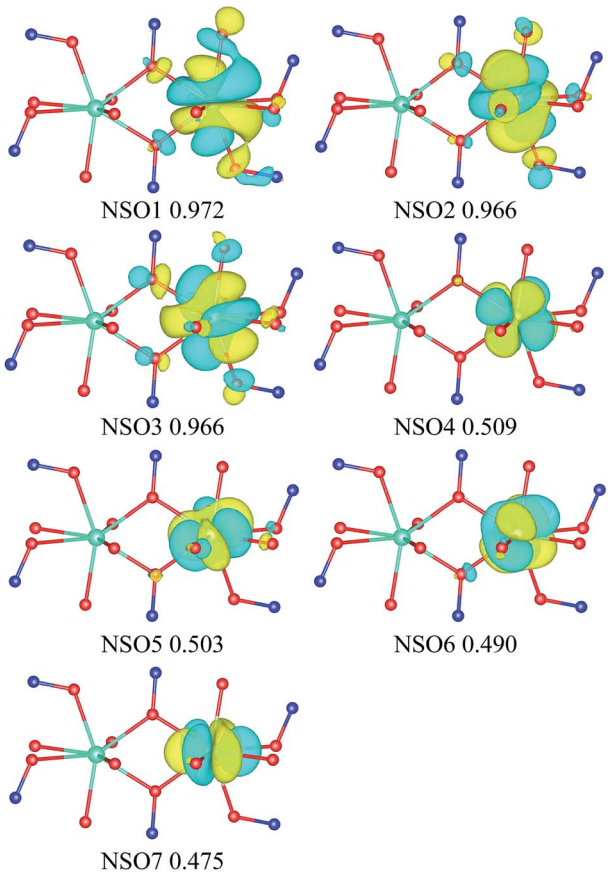

Fig. 5 NSOs for the Dy^{III} complex determined along direction 1 corresponding to the orientation of the magnetization axis. One Dy^{III} has been replaced by a Lu^{III} ion. The isosurfaces are weighted by the corresponding occupation that is indicated below each plot.

The magnetization curve, computed from *ab initio* calculations, does not fit the experimental one. A scaling factor of 1.8 increases the energy of the first excited state and reduces the effect of second order Zeeman interaction (see ESI† for the details of the calculations) and improves the agreement of theoretical and experimental curves, in particular above 1 T. Since the planes of magnetization form a small angle with the intermetallic axis, the dipolar interaction is ferromagnetic. The behavior in the weak field region is reproduced by considering the presence of a supplementary ferromagnetic coupling between the two ions due to exchange ($J_{exch} = +2.4$ cm^{-1}) (Table S9 and Fig. S3†). It is worth noting that when the ground state has a small M_J value and the excited states are close to the ground state as in the present case, a very small error in the energies and in the g_i values may have a dramatic effect on the shape of the magnetization curve. This is why here, a scaling factor that changes the ground-excited state gap was necessary to better reproduce the magnetic data. In addition, if the ratio between g_1 and g_2 is different, the shape of the magnetization curve in the low field region is changed. For instance, if g_1 is close to g_2 (*i.e.* close to 10, which defines an anisotropic easy plane of magnetization), the experimental curve can be reproduced without considering an additional ferromagnetic exchange interaction between the two Er^{III} ions.

In summary, the magnetic studies together with theoretical calculations show that there is an easy axis of magnetization for the Dy and the Tb complexes with an intra-molecular dipolar antiferromagnetic interaction, while for Er there is an easy plane of magnetization that leads to a ferromagnetic dipolar interaction between the two ions. Furthermore, an additional interaction due to exchange between the metal ions is necessary to reproduce the experimental data that was found to be antiferromagnetic for the Dy and the Tb complexes and ferromagnetic (or absent) for the Er one. The analysis of the g values of the ground doublets allow us to extract the spin and the orbital contributions to the overall magnetization (Table S10†).

In order to get a qualitative insight into the nature (F or AF) of the exchange interaction between the metal ions and particularly the difference between the Gd, Tb and Dy complexes on one hand and the Er complex on the other hand, we determined the Natural Spin Orbitals (NSOs) for the magnetic axes on one lanthanide site (Fig. 5, S4 and S5, see ESI†). These orbitals permit the determination of the spin magnetization ('spin density') for a given direction of the magnetic field. The comparison of the overlap integrals between NSOs on different centers within the binuclear complexes for the Dy and the Er cases show that they are about ten times larger for Dy_2Ga_4 then for Er_2Ga_4 (Tables S11, S12 and S13†). Since the overlap integrals between NSOs are directly related to the magnitude of the antiferromagnetic contribution to the exchange interaction,[42] one can conclude that such interaction is expected to be much larger for the Dy_2Ga_4 than for Er_2Ga_4 as found experimentally. The origin of the difference in behavior between the two complexes may be related to the weaker magnetization density on the bridging oxime ligands for

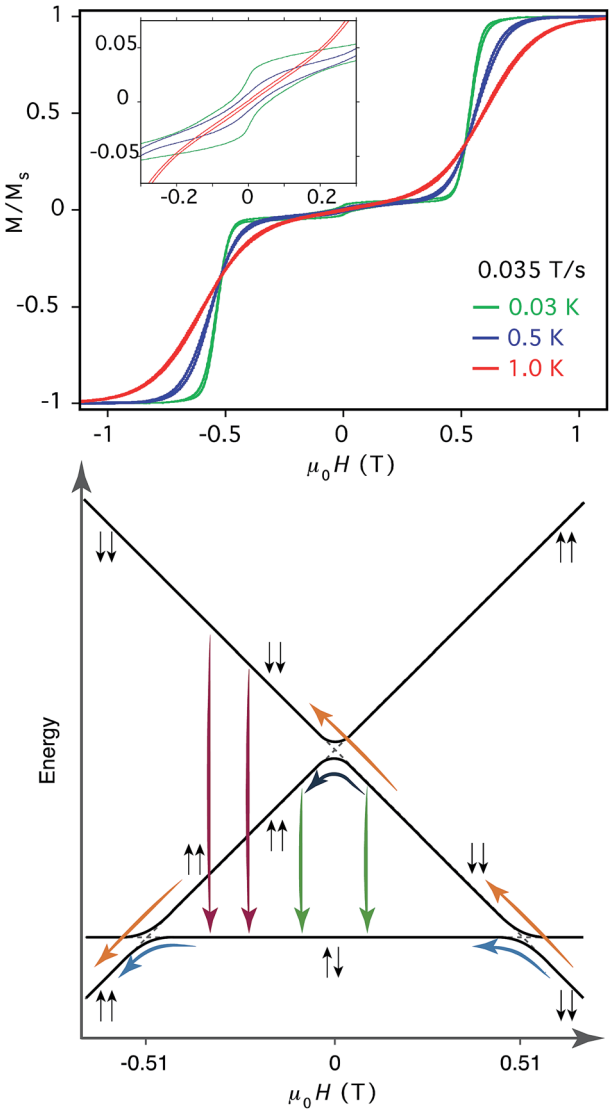

Fig. 6 (top) $M/M_S = c\mu_0 H$) at 0.03, 0.5 and 1 K for dc field sweep rate of 0.035 T s^{-1} for complex 3. (bottom) Field-dependent energy diagram showing the different relaxation processes for the binuclear complex **3**.

Er^{III} than for Dy^{III} (Fig. 5, S4 and S5†). It is difficult to draw more quantitative conclusions from this qualitative analysis on the ferromagnetic exchange contribution.

Low temperature micro-squid studies

For compound **3**, at $\mu_0 H = 1$ T and $T = 0.03$ K, the magnetic moment is saturated. Upon decreasing the field with a sweep rate of 0.035 T s^{-1}, the magnetization undergoes a sharp decrease to around 5% of saturation (Fig. 6, top). The $M = f(\mu_0 H)$ curves at different temperatures cross at 0.51 T. An opening of the hysteresis was observed at zero field with a coercive field $\mu_0 H_C = 540$ Oe. Upon decreasing the magnetic field sweep rate from 0.28 to 0.008 T s^{-1}, the coercive field decreases from 678 to 421 Oe indicating the occurrence of quantum tunneling of the magnetization because the width of the hysteresis loop depends on the field sweep rate (Fig. S6†). The sharp step at 0.51 T is the result of crossover from the F to the AF states as explained in the previous section.

An opening of the hysteresis loop, at such low temperature where only ground state is populated, has never been observed, to the best of our knowledge, in an antiferromagnetically coupled binuclear Dy_2 complex. Since no hysteresis loop can occur when all the molecules are in the antiferromagnetic state (diamagnetic state) and since the excited ferromagnetic one cannot be populated at $T = 0.03$ K, the presence of the residual 5% magnetization below the step at 0.51 T can be due to the

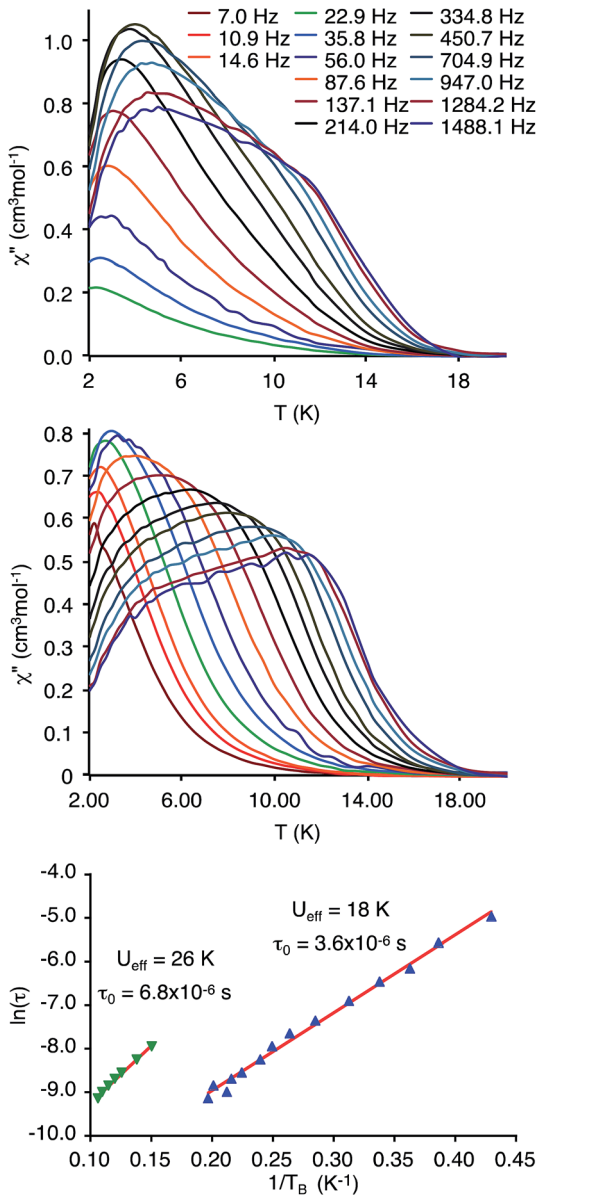

Fig. 7 Temperature-dependence of the out-of-phase (χ'') ac magnetic susceptibility for **3** under zero applied dc field (top) and 2000 Oe (middle); and (bottom) ln(τ) *vs.* $1/T_B$ where T_B Arrhenius plot with data extracted from the frequency-dependent data at zero applied dc field for the low (▲) and the high (▼) temperature processes. The solid lines are the best linear fit.

presence of residual molecules in the ferromagnetic state. Actually, at large positive magnetic field, the moments are in the |– –> configuration of the ferromagnetic state. Upon decreasing the field *at a given sweep rate*, the majority of the molecules undergo a crossover from the ferro- |– –> to the antiferromagnetic (|+ –>; |– +>) state, but a small amount remains in the ferro- |– –> configuration (see Fig. 6, bottom). In order to support the above-proposed mechanism, we first cooled down the sample at zero applied magnetic field. This leads to a state where all Dy-dimers are in the antiferromagnetic ground state. Then, we performed minor hysteresis loops below the critical field for the ferromagnetic state (0.5 T). A typical example is presented in Fig. S6† performed in the ±3000 Oe region. A paramagnetic signal with a small hysteresis is observed, which is probably due to a mononuclear Dy(III) species (2%) that are present in the crystals. Only when the field is larger than the critical field for the ferromagnetic state, a large hysteresis is observed, which is due to molecules that are trapped in the ferromagnetic state.

This results in a residual magnetization below 0.51 T. When the field is driven to zero, a tiny drop in the magnetization is observed (Fig. S7†) that can be assigned to the reversal of the magnetization from the |– –> to the |+ –> (|– +>) configurations by a direct tunneling process (Fig. 6, bottom). The tunneling probability at zero field from |– –> to |+ +> is rather weak but a clear step that is sweep rate dependent can be noticed. Upon decreasing the field to negative values, the reversal of the magnetization occurs probably *via* a direct transition from the |– –> to the |+ –> (|– +>) configuration. And finally at $\mu_0 H = -0.51$ T the majority of the molecules that were in the antiferromagnetic |+ –> (|– +>) state undergo the crossover to the |+ +> ferromagnetic one.

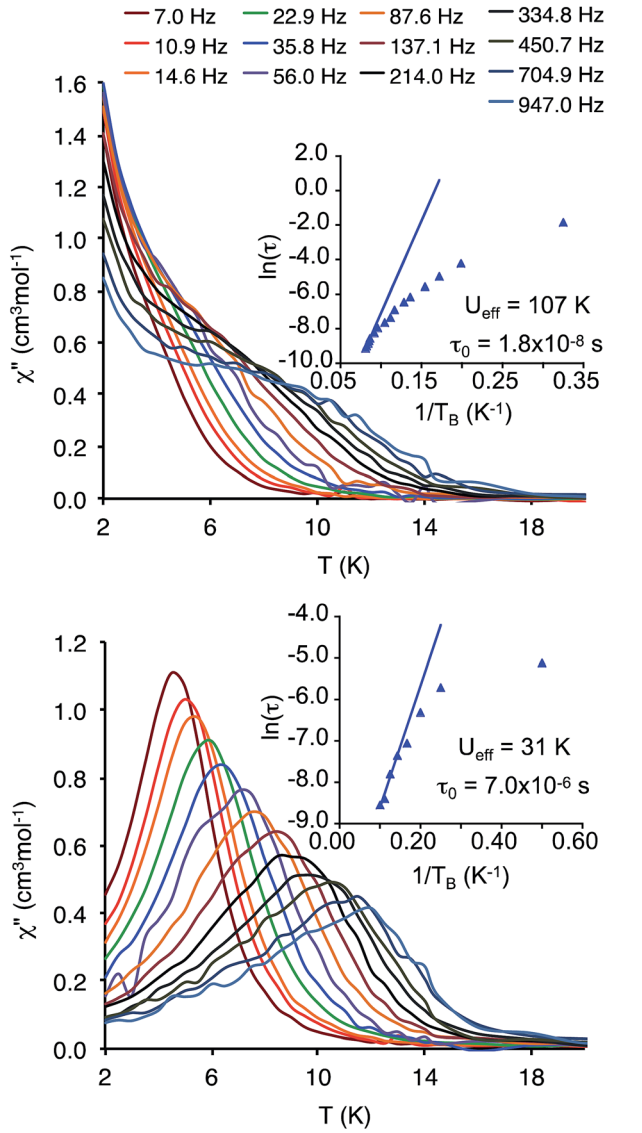

Fig. 8 (top) Temperature-dependence of the out-of-phase (χ'') ac magnetic susceptibility for **6** under zero applied dc field (top) and 750 Oe applied dc field (bottom). Insets: ln(τ) *vs.* $1/T_B$ where T_B is the temperature of the maxima of the χ'' curves.

Dynamic susceptibility studies

Ac susceptibility measurements may bring complementary information on the dynamics of the magnetization reversal at higher temperatures. A frequency dependence of the out-of-phase component of the susceptibility was observed only for the Dy_2 derivative **3** and the Dy diluted one **6**, with all other compounds showing no out-of-phase behavior. For compound **3**, ac susceptibility measurements were first performed under zero dc applied external field, in the temperature range between 2 and 22 K and frequency range from 1 to 1488 Hz with an ac drive field of 3 Oe (Fig. 7 (top), S8 and S9†).

The temperature dependent out-of-phase susceptibility plot (Fig. 7, top) show that upon increasing the frequency of the oscillating field, the temperature of the maxima (T_{Bf}) shifts toward high temperatures as expected, while the value of the maxima of the χ'' signals does not behave as usual. When the frequency increases, it first reaches a maximum intensity at 450 Hz (T_{B450} = 4.00 K) and then decreases. This behavior is

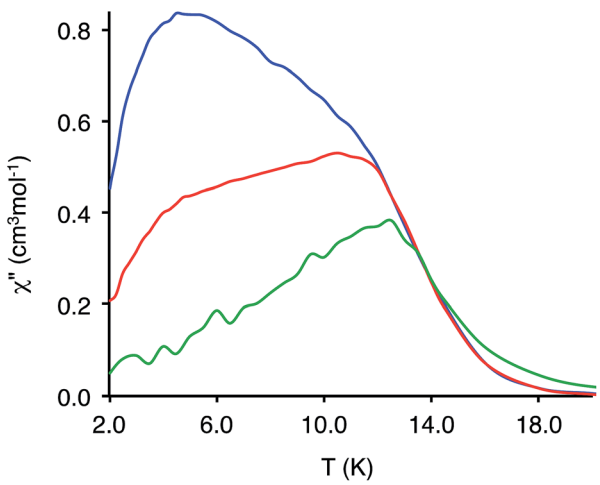

Fig. 9 Temperature-dependence of the out-of-phase (χ'') ac susceptibility for **3** in zero dc field (—), in 2000 Oe dc field (—) and for **6** in 750 Oe dc field (—) at 1284 Hz.

consistent with the fact that the slow relaxation probed corresponds to an excited state that is more and more populated when the temperature of the maximum is shifted upward and is evidence that the relaxation process observed is due to the excited ferromagnetic state that lies at 4.9 cm^{-1} above the ground non-magnetic one. Assuming an activated relaxation process ($\tau = \tau_0 \exp(U_{eff}/k_B T_B)$) in the 2–5 K region, it is possible to fit ln τ *vs.* $1/T_B$ from the out-of phase data, where $\tau = 1/(2\pi f)$ and T_B is the temperature of the $\chi'' = f(T)$ curves, and find $\tau_0 = 3.6 \times 10^{-6}$ s and $U_{eff} = 18$ K (Fig. 7, bottom). The $\chi'' = f(T)$ curves display shoulders at higher temperatures in the 10–14 K region that appear only for frequencies above 500 Hz. In the 10–14 K region, the temperature is larger than the energy due to antiferromagnetic coupling, the coupling can then be neglected and the ions behave as if they were isolated. This second relaxation process can then be assigned to the isolated Dy^{III} ions. The analysis of the data leads to a thermal activated behavior relaxation process with $\tau_0 = 6.8 \times 10^{-6}$ s and $U_{eff} = 26$ K (Fig. 7, bottom).

The $\chi'' = f(\nu)$ curves for different temperatures (Fig. S8†) show only one maximum that shifts to high frequency upon heating. The intensity of the curves follow the behavior observed in Fig. 7 *i.e.* the magnitude of χ'' increases from 2 to 4.25 K and then decreases, attesting that the relaxation process is due to the excited ferromagnetic state.

The Cole–Cole plots for compound **3** at zero applied dc field were obtained for temperatures between 2 and 11 K (Fig. S10†). The plots have close to an ideal semicircular shape indicating that only a few relaxation processes are present. The semicircles were fitted using a generalized Debye model.[43] The fits provided values for the α parameter, which decreased with increasing temperature, from 0.18 at 2 K to 0.032 at 11 K (Fig. S10†). The low α value at high temperatures indicates that only one relaxation process is present. As the temperature is decreased, the α parameter increases because at low temperatures, the tunneling process starts to compete with the activated direct process.

The ac data for compound **3** were also recorded in the presence of an applied 2000 Oe dc field. The same general behavior with two relaxation processes, as for the zero dc field case, is observed, but with some differences in the relative intensities. (Fig. 7 (middle) and S11†). Upon increasing the frequency, the intensity of χ'' increases and reaches a maximum at 36 Hz ($T_{B36} = 3.0$ K), instead of 450 Hz under zero dc field. The high temperature process starts to be observable at 88 Hz instead of 450 Hz when a dc field of 2000 Oe is applied, which is compatible with a process due to the uncoupled Dy^{III} ions.

The temperature-dependent out-of-phase ac susceptibility for **6** under zero dc applied field (Fig. 8 top and S12†) revealed a frequency dependent maxima in the 5–15 K temperature range with a tail at low temperature due to quantum tunneling of the magnetization, as is generally observed for Dy^{III} ions.[44] This last process can also be observed in the low temperature regime in the frequency-dependent data (Fig. S13†), where the maxima positions are relatively temperature independent. The barrier extracted from the frequency-dependent data for **6** at zero applied dc field is $U_{eff} = 31$ K, with a τ_0 of 7.0×10^{-6} s (Fig. 8 top), very close to the high temperature process of the binuclear compound **3** ($U_{eff} = 26$ K and $\tau_0 = 76.8 \times 10^{-6}$ s), which confirms that the high temperature process in **3** is indeed due to the uncoupled moments. At lower temperature, the relaxation tends to be temperature independent (Fig. 8, top), as expected when the quantum tunneling process dominates.

Applying a dc magnetic field may slow down the tunneling and make other processes more visible. In the presence of an optimal 750 Oe dc field (see ESI, Fig. S14†), the maxima in the $\chi'' = f(T)$ plot for **6** can be observed (Fig. 8, bottom). Quantum tunneling of the magnetization has been mostly quenched as evidenced by the absence of overlapping peaks in the frequency-dependent data (Fig. S15†) and the disappearance of the low temperature tail in the temperature dependent data (Fig. 8).

A linear fit of the high temperature data gives an energy barrier $U_{eff} = 107$ K, with $\tau_0 = 1.79 \times 10^{-8}$ s (Fig. 8, bottom). As expected, the barrier is much higher than for the zero-field case of 31 K. It is about half the value of the computed energy difference between the ground and the first excited states (153 cm^{-1} (220 K)) (Table S4†), which is consistent with the persistence of a relaxation by quantum tunneling *via* the ground state and *via* the first excited one. The persistence of quantum tunneling is due to the lack of a perfect axial *g*-tensor ($g_1 = 19.47$, $g_2 = 0.08$ and $g_3 = 0.04$) and thus to a small mixing between the ground and the excited M_J states.

The comparison of the χ'' curves at 1284 Hz measured at zero and 2000 Oe for **3** and at 750 Oe for **6** (Fig. 9) shows that the maximum of $\chi'' = f(T)$ for **3** and **6** are at the same temperature, which confirms that the high temperature process in **3** is actually due to the isolated Dy^{III} ions.

In order to check that the relaxation processes are well related to the mononuclear DyY species and not to the presence of large amounts of the Dy_2 ones within the crystal, we carried magnetization studies on a single crystal of compound **6** using the micro-squid arrays. The $M = f(\mu_0 H)$ curves in the ± 1 T range at different temperatures and sweep rates (Fig. S16 and S17†) of the field are all consistent with a mononuclear Dy(III) ion with a tunneling of the magnetization near zero field and a slower relaxation when a magnetic field is applied, completely consistent with the ac data. A small step is observed close to 0.5 T due to the Dy_2 species present in compound **6**. The corresponding magnetization is around 6%, which is less than the value expected from statistical distribution (11%), which render the magnetic behavior of compound **6** mainly due to the mononuclear species.

Concluding remarks

Utilizing the metallacrown synthetic approach, we investigated the properties of a family of isostructural Ln_2Ga_4 complexes, where the Ln^{III} ions are bridged by oxygen atoms forming the diamond-like Ln_2O_2 core. The experimentally observed antiferromagnetic coupling for the Gd, Tb and Dy containing complexes was shown, using *ab initio* calculations, to be due to exchange and not to dipolar interaction. For the Er-based complex, no experimental evidence of antiferromagnetic coupling was observed. The analysis of the overlap and the exchange integrals between the NSOs shows that the exchange

coupling is about ten times larger for Dy than for Er. The magnetization changes from an easy axis to an easy plane between the Dy and the Er complexes but there is no evidence that this is related to the nature of the exchange interaction.

The presence of an easy axis of magnetization for the Dy^{III} within the binuclear species leads to a slow relaxation of the magnetization for Dy_2, despite the presence of the antiferromagnetic coupling. Two relaxation processes are observed and assigned to the ferromagnetic excited state and to the uncoupled ions. The uncoupled ions have a slightly larger barrier suggesting that the ferromagnetic coupling between the Ising moments speeds up the relaxation process. The nature of the high temperature process was confirmed by the study of the diluted mononuclear species.

Acknowledgements

This research was supported in part by the National Science Foundation under grant CHE-1361779 and by ANR-13-BS10-0001-03 MolQuSpin. VLP and TM acknowledge the Blaise Pascal International Chair for financial support. F.G. and J.A. acknowledge support Department of Energy, Office of Basic Energy Sciences, Heavy Element Chemistry (DE-FG02-09ER16066). The SQUID facility at the University of Michigan is funded by the National Science Foundation, NSF-MRI grant CHE-1040008.

Notes and references

‡ The successive deprotonation of salicylhydroxamic acid is as follows: H_3shi (fully protonated), H_2shi^- (deprotonation of the hydroximate oxygen), $Hshi^{2-}$ (deprotonation of the hydroximate and phenol oxygens) and shi^{3-} (fully deprotonated).

§ Theoretical calculations estimate that single ion anisotropy lifts the degeneracy of the local $S = 7/2$ manifold by 2 cm^{-1} (Table S2†). The evaluation of the dipolar interaction from *ab initio* calculations leads to an energy separation between the ground and the highest excited state of about 0.4 cm^{-1}, which is about 10% of the overall separation.

¶ The principal values of the g tensor for all compounds are labeled by **1**, **2** and **3** with **1** being the largest and **3** the smallest value; the molecular axes x, y and z; the z axis corresponds to the Ln–Ln intermolecular axis and the x axis lies within the LnOOLn plane, where O are the bridging oxygen atoms.

1 R. Sessoli, H. Tsai, A. R. Schake, S. Wang, J. B. Vincent, K. Folting, D. Gatteschi, G. Christou and D. N. Hendrickson, *J. Am. Chem. Soc.*, 1993, **115**, 1804.
2 L. Bogani and W. Wernsdorfer, *Nat. Mater.*, 2008, **7**, 179.
3 R. E. P. Winpenny, *Angew. Chem., Int. Ed.*, 2008, **47**, 7992.
4 C. M. Zaleski, E. C. Depperman, C. Dendrinou-Samara, M. Alexiou, J. W. Kampf, D. P. Kessissoglou, M. L. Kirk and V. L. Pecoraro, *J. Am. Chem. Soc.*, 2005, **127**, 12862.
5 A. M. Ako, I. J. Hewitt, V. Mereacre, R. Clérac, W. Wernsdorfer, C. E. Anson and A. K. Powell, *Angew. Chem., Int. Ed.*, 2006, **45**, 4926; G. Christou, D. Gatteschi, D. N. Hendrickson and R. Sessoli, *MRS Bull.*, 2000, **25**, 66; A. L. Barra, A. Caneschi, A. Cornia, F. Fabrizi de Biani, D. Gatteschi, C. Sangregorio, R. Sessoli and L. Sorace, *J. Am. Chem. Soc.*, 1999, **121**, 5302.
6 C. M. Zaleski, S. Tricard, E. C. Depperman, W. Wernsdorfer, T. Mallah, M. L. Kirk and V. L. Pecoraro, *Inorg. Chem.*, 2011, **50**, 11348.
7 D. N. Woodruff, R. E. P. Winpenny and R. A. Layfield, *Chem. Rev.*, 2013, **113**, 5110.
8 N. Ishikawa, M. Sugita, T. Ishikawa, S. Koshihara and Y. Kaizu, *J. Am. Chem. Soc.*, 2003, **125**, 8694; V. E. Campbell, R. Guillot, E. Riviere, P.-T. Brun, W. Wernsdorfer and T. Mallah, *Inorg. Chem.*, 2013, **52**, 5194; D.-P. Li, T.-W. Wang, C.-H. Li, D.-S. Liu, Y.-Z. Li and X.-Z. You, *Chem. Commun.*, 2010, **46**, 2929; A. Yamashita, A. Watanabe, S. Akine, T. Nabeshima, M. Nakano, T. Yamamura and T. Kajiwara, *Angew. Chem., Int. Ed.*, 2011, **50**, 4016; A. Watanabe, A. Yamashita, M. Nakano, T. Yamamura and T. Kajiwara, *Chem.–Eur. J.*, 2011, **17**, 7428; N. Zhou, Y. Ma, C. Wang, G. Feng Xu, J.-K. Tang, J.-X. Xu, S.-P. Yan, P. Cheng, L.-C. Li and D.-Z. Liao, *Dalton Trans.*, 2009, 8489; M. A. AlDamen, J. M. Clemente-Juan, E. Coronado, C. Martí-Gastaldo and A. Gaita-Ariño, *J. Am. Chem. Soc.*, 2008, **130**, 8874.
9 L. F. Chibotaru, L. Ungur and A. Soncini, *Angew. Chem., Int. Ed.*, 2008, **47**, 4126.
10 R. Boča, *Coord. Chem. Rev.*, 2004, **248**, 757.
11 R. J. U. Blagg, L. Ungur, F. Tuna, J. Speak, P. Comar, D. Collison, W. Wernsdorfer, E. J. L. McInnes, L. F. Chibotaru and R. E. P. Winpenny, *Nat. Chem.*, 2013, **5**, 673.
12 W. Wernsdorfer, N. Aliaga-Alcalde, D. N. Hendrickson and G. Christou, *Nature*, 2002, **416**, 406.
13 J. D. Rinehart, M. Fang, W. J. Evans and J. R. Long, *J. Am. Chem. Soc.*, 2011, **133**, 14236.
14 R. J. Blagg, C. A. Muryn, E. J. L. McInnes, F. Tuna and R. E. P. Winpenny, *Angew. Chem., Int. Ed.*, 2011, **50**, 6530; Y.-N. Guo, G.-F. Xu, P. Gamez, L. Zhao, S.-Y. Lin, R. Deng, J. Tang and H.-J. Zhang, *J. Am. Chem. Soc.*, 2010, **132**, 8538.
15 P.-H. Lin, T. J. Burchell, L. Ungur, L. F. Chibotaru, W. Wernsdorfer and M. Murugesu, *Angew. Chem., Int. Ed.*, 2009, **48**, 9489.
16 F. Habib and M. Murugesu, *Chem. Soc. Rev.*, 2013, **42**, 3278; F. Tuna, C. A. Smith, M. Bodensteiner, L. Ungur, L. F. Chibotaru, E. J. L. McInnes, R. E. P. Winpenny, D. Collison and R. A. Layfield, *Angew. Chem., Int. Ed.*, 2012, **51**, 6976; M. Nematirad, W. J. Gee, S. K. Langley, N. F. Chilton, B. Moubaraki, K. S. Murray and S. R. Batten, *Dalton Trans.*, 2012, 13711; K. Katoh, Y. Horii, N. Yasuda, W. Wernsdorfer, K. Toriumi, B. K. Breedlove and M. Yamashita, *Dalton Trans.*, 2012, 13582.
17 S. A. Sulway, R. A. Layfield, F. Tuna, W. Wernsdorfer and R. E. P. Winpenny, *Chem. Commun.*, 2012, **48**, 1508.
18 G. Mezei, C. M. Zaleski and V. L. Pecoraro, *Chem. Rev.*, 2007, **107**, 4933.
19 C. M. Zaleski, E. C. Depperman, J. W. Kampf, M. L. Kirk and V. L. Pecoraro, *Angew. Chem., Int. Ed.*, 2004, **43**, 3912; C. M. Zaleski, E. C. Depperman, J. W. Kampf, M. L. Kirk and V. L. Pecoraro, *Inorg. Chem.*, 2006, **45**, 10022; A. Deb, T. T. Boron, M. Itou, Y. Sakurai, T. Mallah, V. L. Pecoraro and J. E. Penner-Hahn, *J. Am. Chem. Soc.*, 2014, **136**, 4889.

20 C. M. Zaleski, J. W. Kampf, T. Mallah, M. L. Kirk and V. L. Pecoraro, *Inorg. Chem.*, 2007, **46**, 1954.
21 I. T. T. Boron, J. W. Kampf and V. L. Pecoraro, *Inorg. Chem.*, 2010, **49**, 9104.
22 (*a*) J. Tang, I. Hewitt, N. T. Madhu, G. Chastanet, W. Wernsdorfer, C. E. Anson, C. Benelli, R. Sessoli and A. K. Powell, *Angew. Chem., Int. Ed.*, 2006, **45**, 1729; (*b*) X. H. Yi, K. Bernot, F. Pointillart, G. Poneti, G. Calvez, C. Daiguebonne, O. Guillou and R. Sessoli, *Chem. Eur. J.*, 2012, **18**, 11379; (*c*) F. Pointillart, B. Le Guennic, O. Maury, S. Golhen, O. Cador and L. Ouahab, *Inorg. Chem.*, 2013, **52**, 1398.
23 Bruker Analytical X-ray, Madison, WI, 2008.
24 G. M. Sheldrick, *Program for Empirical Absorbtion Correction of Area Detector Data*, Gottingen, Germany, 2008.
25 R. Corporation, Tokyo, Japan.
26 G. M. Sheldrick, *Acta Crystallogr., Sect. A: Found. Crystallogr.*, 2008, **64**, 112.
27 W. Wernsdorfer, *Supercond. Sci. Technol.*, 2009, **22**, 064013.
28 W. Wernsdorfer, N. E. Chakov and G. Christou, *Phys. Rev. B: Condens. Matter Mater. Phys.*, 2004, **70**, 132413.
29 B. O. Roos, R. Lindh, P.-Å. Malmqvist, V. Veryazov, P.-O. Widmark and A. C. Borin, *J. Phys. Chem. A*, 2008, **112**, 11431; B. O. Roos, R. Lindh, P.-Å. Malmqvist, V. Veryazov and P.-O. Widmark, *J. Phys. Chem. A*, 2003, **108**, 2851.
30 F. Aquilante, L. De Vico, N. Ferré, G. Ghigo, P.-Å. Malmqvist, P. Neogrády, T. B. Pedersen, M. Pitoňák, M. Reiher, B. O. Roos, L. Serrano-Andrés, M. Urban, V. Veryazov and R. Lindh, *J. Comput. Chem.*, 2010, **31**, 224.
31 B. O. Roos, P. R. Taylor and P. E. M. Siegbahn, *Chem. Phys.*, 1980, **48**, 157.
32 P.-Å. Malmqvist, B. O. Roos and B. Schimmelpfennig, *Chem. Phys. Lett.*, 2002, **357**, 230.
33 B. A. Heß, C. M. Marian, U. Wahlgren and O. Gropen, *Chem. Phys. Lett.*, 1996, **251**, 365.
34 H. Bolvin, *ChemPhysChem*, 2006, **7**, 1575.
35 M. E. Lines, *J. Chem. Phys.*, 1971, **55**, 2977.
36 M. L. Kahn, R. Ballou, P. Porcher, O. Kahn and J.-P. Sutter, *Chem.–Eur. J.*, 2002, **8**, 525.
37 S. Petit, G. Pilet, D. Luneau, L. F. Chibotaru and L. Ungur, *Dalton Trans.*, 2007, 4582.
38 F. Gendron, D. Páez-Hernández, F.-P. Notter, B. Pritchard, H. Bolvin and J. Autschbach, *Chem.–Eur. J.*, 2014, **20**, 7994.
39 J. Jankolovits, C. M. Andolina, J. W. Kampf, K. N. Raymond and V. L. Pecoraro, *Angew. Chem., Int. Ed.*, 2011, **50**, 9660; S. H. Seda, J. Janczak and J. Lisowski, *Inorg. Chem. Commun.*, 2006, **9**, 792.
40 J. r. m. Long, F. Habib, P.-H. Lin, I. Korobkov, G. Enright, L. Ungur, W. Wernsdorfer, L. F. Chibotaru and M. Murugesu, *J. Am. Chem. Soc.*, 2011, **133**, 5319.
41 L. E. Roy and T. Hughbanks, *J. Am. Chem. Soc.*, 2006, **128**, 568.
42 P. W. Anderson, in *Magnetism*, ed. G. T. R. Suhl, Academic Press, 1963, p. 25; J.-J. Girerd, M.-F. Charlot and O. Kahn, *Mol. Phys.*, 1977, **34**, 1063; O. Kahn, *Molecular Magnetism*, VCH Publishers, Inc., New York, 1993.
43 N. Bontemps, J. Rajchenbach, R. V. Chamberlin and R. Orbach, *Phys. Rev. B: Condens. Matter Mater. Phys.*, 1984, **30**, 6514; D. Huser, A. J. v. Duyneveldt, G. J. Nieuwenhuys and J. A. Mydosh, *J. Phys. C: Solid State Phys.*, 1986, **19**, 3697.
44 J. J. Le Roy, M. Jeletic, S. I. Gorelsky, I. Korobkov, L. Ungur, L. F. Chibotaru and M. Murugesu, *J. Am. Chem. Soc.*, 2013, **135**, 3502.